
EFFECTIVE MAGNETIC DIPOLAR ANISOTROPY IN NANOMAGNETS: EQUILIBRIUM MAGNETIZATION STATES

V.P. KRAVCHUK, D.D. SHEKA

UDC 537.611
© 2008

Taras Shevchenko Kyiv National University
(2 Build. 5, Academician Glushkov Ave., Kyiv 03127, Ukraine; e-mail: waldemar@univ.kiev.ua)

Equilibrium magnetization states of thin nanoparticles of various forms are studied theoretically, using the approximation of the effective anisotropy caused by the magnetic dipolar interaction. The magnetization distributions near a plane angle and for dots, which have form of regular polygons, are predicted theoretically for magnets with weak exchange interaction. The sizes of magnetization inhomogeneities near the angle vertex are estimated theoretically. The analytic results are in a good agreement with the results of micromagnetic simulations for square prisms.

1. Introduction

In recent years, a growing interest in the study of static and dynamic properties of nm-sized magnetic particles. This interest is caused by unusual physical properties of objects and various practical applications [1–3]. Magnetic properties of nanoparticles are well described in the macrospin approximation [4] only if the size of a particle does not exceed 10 nm [1]. For particles of a greater size, the ground state stops to be homogeneous. In magnetics, there appear the domain structures whose characteristic size is determined by the “magnetic length” $l = \sqrt{A/K}$ (A is the exchange interaction constant, and K is the single-ion anisotropy constant). Magnetic anisotropy is a reason for the appearance of a domain structure in massive specimens. In small particles made of magnetically soft materials with a small factor of quality $Q = K/4\pi M_s^2 \ll 1$ (M_s is the saturation magnetization), the magnetic dipolar interaction turns out to be the dominant mechanism of appearance of a domain structure [1, 5]: the typical “exchange length” $\ell = \sqrt{A/4\pi M_s^2}$ is about 5–10 nm for typical magnetically soft materials.

Inhomogeneous states in such magnetics, in particular a domain structure, are determined, in the first turn, by the form of a magnet. The reason for such states to appear is the anisotropy of a form which is due to the magnetic dipolar interaction [5]. In particular, the plane-parallel distribution of the magnetization with magnetic flux closure patterns is observed in the magnetic elements of μm -sized thin films [1]. The magnetization distribution in such structures is described by the van den Berg method [6–9]. The idea consists in the determination of a two-dimensional (plane-parallel) magnetization field ensuring the full absence of a demagnetization field, which is possible only in the absence of bulk ($\vec{\nabla} \cdot \vec{M} = 0$) and surface ($\vec{M} \cdot \vec{n} = 0$) magnetostatic charges. It was shown in [6–9] with the use of the methods of differential geometry that, for a one-connected region, a corresponding solenoidal distribution of the magnetization is possible only under the appearance of a domain structure. It is worth noting that the van den Berg domains do not include a thin structure (the zero thickness of a domain wall) due to the neglect of the exchange interaction. Though the idealized model of van den Berg explains the reason for the appearance of inhomogeneous states in elements of magnetically soft films of micron size, it stops to be valid for smaller systems of submicron size due to the possible turning of the magnetization vector from the plane, the inhomogeneous distribution over thickness, etc. [10]. But just particles of submicron size are actual now for numerous applications. In particular, in particles of the disk form, the ground state can be vortex one [1, 11]. Particles in the vortex state are promising candidates for fast gages of magnetic fields and data-storage devices

with high density [11] and for the study of fundamental properties of magnetic substances.

As was already noted, the basic reason for an inhomogeneity of the magnetization distribution in magnetically soft nanomagnetics is the magnetic dipolar interaction, whose account is the necessary condition for the adequate description of inhomogeneous structures of the magnetization. The nonlocal character of the magnetic dipolar interaction significantly complicates the theoretical analysis of properties of magnetic nanostructures which is usually performed numerically, e.g., with the use of micromagnetic modeling [12]. By now, the analytic analysis of the magnetic dipolar interaction was carried out for certain limiting relations between the parameters of a system: the length L , thickness h , and exchange length ℓ . In particular, it was proved in [13] that, for infinitely thin films under the conditions $h/L \rightarrow 0$ and $\ell/L \rightarrow \text{const}$, the magnetostatic energy has a local form of the anisotropy energy of the “easy plane” type; in this case, the homogeneous ground state is realized in the plane of a film. The magnetostatic interpretation of the mentioned effective anisotropy is reduced to the influence of surface magnetostatic charges: the surface charges along a film create a magnetostatic capacitor with energy $2\pi M_s^2$ [14]. The magnetostatic charges of the edge surface cause the surface anisotropy [14–16] that leads to the appearance of surface nonlinear excitations, in particular, half-vortices or boojums [17–19]. The analytic description of the effective anisotropy caused by the magnetic dipolar interaction was constructed recently in work [20] for magnetics of finite thickness under the conditions

$$h/L \ll 1, \quad \ell/L \ll 1. \quad (1)$$

In this approach, it is assumed that the magnetization $\vec{M} = M_s(\sin \theta \cos \phi, \sin \theta \sin \phi, \cos \theta)$ depends only on the coordinates (ρ, χ) in the plane of a magnet. Such plane-parallel distribution of the magnetization is adequate for magnetics of constant thickness under conditions (1). According to [20], the energy of the magnetic dipolar interaction looks as

$$E = \pi M_s^2 h \int W d^2x,$$

$$W = \mathcal{A}[1 - 3 \cos^2 \theta] + \sin^2 \theta \operatorname{Re} \left[\mathcal{B} e^{2i(\phi - \chi)} \right]. \quad (2)$$

The quantities $\mathcal{A} \equiv \mathcal{A}(\rho, \chi)$ and $\mathcal{B} \equiv \mathcal{B}(\rho, \chi)$ are functions of the coordinates and determine the

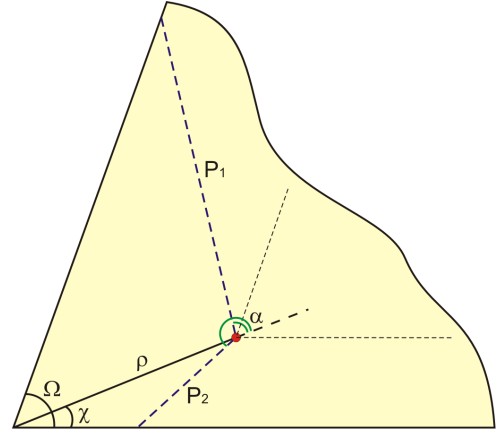


Fig. 1. Designations for the calculation of the effective anisotropy for an angle

coefficients of spatially inhomogeneous anisotropy:

$$\mathcal{A} = \frac{1}{2\pi} \int_0^{2\pi} G(P/h) d\alpha - \frac{2}{3}, \quad G(x) = \sqrt{x^2 + 1} - x, \quad (3a)$$

$$\mathcal{B} = -\frac{1}{2\pi} \int_0^{2\pi} [G(P/h) + 2 \ln G(h/P)] e^{-2i\alpha} d\alpha. \quad (3b)$$

Here, $P \equiv P(\rho, \chi|\alpha)$ denotes the distance from a point (ρ, χ) to the lateral surface of a specimen in the direction α (see Fig. 1).

It is worth noting that the form of the functions $\mathcal{A}(\rho, \chi)$ and $\mathcal{B}(\rho, \chi)$ is completely determined by the size and form of a specimen. In this case, h plays the role of a length unit. The coefficient \mathcal{A} is real-valued in all the cases and plays the role of the constant of effective uniaxial anisotropy (directed normally to the plane of a specimen). Under the conditions $\mathcal{A} > 0$ and $\mathcal{A} < 0$, the anisotropies of the “easy axis” and “easy plane” are realized, respectively. We note that, for thin specimens, we have always the easy-plane anisotropy [20]. In thin specimens where the magnetization lies mainly in the XY -plane, the direction ϕ in the plane is determined by the second term in the formula for the energy in (2), namely by the expression $\operatorname{Re}[\mathcal{B} e^{2i(\phi - \chi)}]$. By minimizing the energy, this direction is determined as

$$\phi(\rho, \chi) = \chi + \frac{\pi}{2} - \frac{1}{2} \operatorname{Arg} \mathcal{B}(\rho, \chi). \quad (4)$$

We now consider the lines of effective anisotropy, the tangents to which at points (ρ, χ) have the slope angle

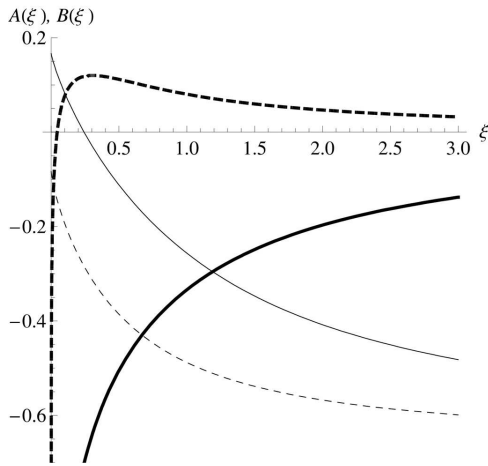


Fig. 2. Dependences $\mathcal{A}(\xi)$ (thin line) and $\mathcal{B}(\xi)$ (bold line) along the bisectrix for different values of the angle Ω : solid line – $\Omega = \pi/3$, dashed line – $\Omega = 5\pi/6$

$\phi(\rho, \chi)$ [20]. These lines determine the magnetization distribution for a purely two-dimensional distribution and the neglect by both the exchange interaction and the single-ion anisotropy. We note that, at large distances from the surface (the quantity $|\mathcal{B}|$ tends to 0 with increase in the distance from the surface, see Fig. 2 and Fig. 2b in [20]), the calculation of the magnetization distribution requires to account all magnetic interactions. In this case, the lines of effective anisotropy are a means to approximately account the magnetostatic interaction as a local one. But, as was shown in work [20], the method describes very precisely the magnetization distribution in inhomogeneous states of real nanomagnetics under conditions (1).

In the present work within the indicated approach, we study the magnetization distribution in magnetics of various geometries. In this case, we neglect specific features of the surface layer of a magnetic, by assuming that the state of magnetic ions of the surface layer does not differ from the state of internal ions. In Section 2, we study the distribution of the lines of effective anisotropy near a planar angle. The results are generalized to the analysis of such a distribution in magnetics that have form of regular polygons (Section 3). In Section 4, we analyze the size of inhomogeneities near the vertices of angles.

2. Effective Anisotropy Near a Planar Angle

We now consider an infinite plane ferromagnetic plate with thickness h which has the form of an angle $\angle\Omega$ (see Fig. 1). In this case, the distances P_1 and P_2 to the angle

sides are defined as

$$P_1(\rho, \chi|\alpha) = \frac{\rho \sin(\Omega - \chi)}{\sin(\chi + \alpha - \Omega)}, \quad P_2(\rho, \chi|\alpha) = -\frac{\rho \sin(\chi)}{\sin(\chi + \alpha)}.$$

Let us consider the behavior of the effective anisotropy along the angle bisectrix $\chi = \Omega/2$. The calculation by formulas (3) indicates that the coefficients \mathcal{A} and \mathcal{B} are real-valued along the angle bisectrix:

$$\mathcal{A} = \frac{1}{\pi} \int_{\Omega/2}^{\pi} G(P/h) d\alpha - \frac{2}{3},$$

$$\mathcal{B} = -\frac{1}{\pi} \int_{\Omega/2}^{\pi} \cos 2\alpha [G(P/h) + 2 \ln G(h/P)] d\alpha,$$

$$P \equiv P_1(\bullet|\alpha) = P_2(\bullet|-\alpha) = \frac{\rho \sin \Omega/2}{\sin(\alpha - \Omega/2)}. \quad (5)$$

According to (4), the lines of effective anisotropy are parallel to the bisectrix at $\mathcal{B} < 0$ and normal to it at $\mathcal{B} > 0$. At the point of the bisectrix, where $\mathcal{B} = 0$, we have a saddle point. Moreover, the density of the linear part of the magnetostatic energy at this point will not depend on the orientation of the magnetization in the plane of a specimen ϕ . The straightforward calculation of expressions (5) for angles $\Omega \in (0; \pi)$ gives

$$\begin{aligned} \mathcal{A}(\xi) = & -\frac{1}{\pi} \left[\text{arctg} \left(\xi \sin \frac{\Omega}{2} \right) + \text{arctg} \left(\sqrt{1 + \xi^2} \text{tg} \frac{\Omega}{2} \right) + \right. \\ & \left. + \xi \sin \frac{\Omega}{2} \ln \frac{\sqrt{1 + \xi^2} - \xi \cos \frac{\Omega}{2}}{2\xi \sin^2 \frac{\Omega}{4}} \right] + \frac{1}{3}, \\ \mathcal{B}(\xi) = & -\frac{3}{4} \cos \Omega + \frac{\cos \Omega}{\pi} \left[\text{arctg} \left(\xi \sin \frac{\Omega}{2} \right) + \right. \\ & \left. + \frac{1}{2} \text{arctg} \frac{\xi^2 \text{tg} \frac{\Omega}{2} - 2 \text{ctg} \Omega}{2\sqrt{1 + \xi^2}} - \right. \\ & \left. - \xi \sin \frac{\Omega}{2} \ln \frac{2\xi \sin^2 \frac{\Omega}{4} (\sqrt{1 + \xi^2} + \xi \cos \frac{\Omega}{2})}{1 + \xi^2 \sin^2 \frac{\Omega}{2}} \right] + \\ & \left. + \frac{\sin \Omega}{\pi} \left[\sqrt{1 + \xi^2} - \xi + \ln \frac{\xi}{\sqrt{1 + \xi^2} + 1} \right], \end{aligned}$$

where $\xi = \rho/h$. The dependence $\mathcal{A}(\xi)$ is always monotonously decreasing (see Fig. 2). The dependence

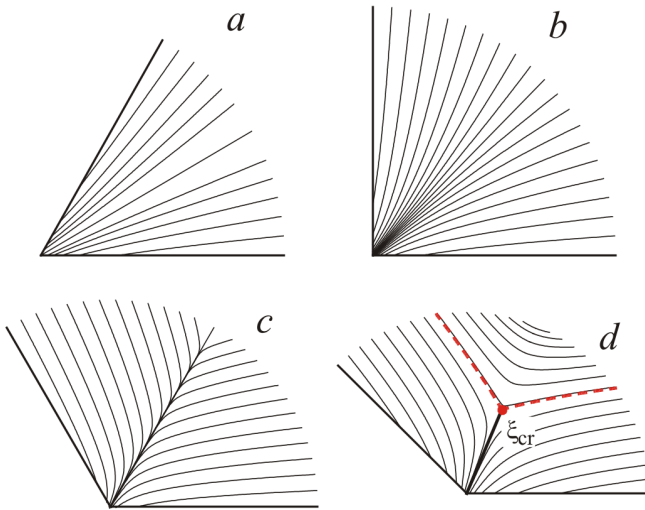


Fig. 3. Distribution of the lines of effective anisotropy for different angles: $a: \Omega = \pi/3$, $b: \Omega = \pi/2$, $c: \Omega = 2\pi/3$, $d: \Omega = 3\pi/4$

$\mathcal{B}(\xi)$ qualitatively changes its form on the passage through the critical value

$$\Omega_{\text{cr}} = \frac{2\pi}{3}. \quad (6)$$

For angles $\Omega \in (0; \Omega_{\text{cr}})$, the function $\mathcal{B}(\xi)$ takes only negative values and monotonously increases. However, at $\Omega \in (\Omega_{\text{cr}}; \pi)$, there appears a maximum of the dependence $\mathcal{B}(\xi)$. In this case, the function changes its sign at some value ξ_{cr} (see Fig. 2). Calculating numerically the coefficient $\mathcal{B}(\rho, \chi)$ for the whole area of the angle by formula (3b), we can construct a characteristic distribution of the lines of effective anisotropy for various angles (see Fig. 3). The main peculiarity of angles $\Omega \in (\Omega_{\text{cr}}; \pi)$ is the appearance of a saddle point on the bisectrix which is shown in Fig. 3, d as a circle.

The position of a saddle point ξ_{cr} is determined by the condition $\mathcal{B}(\xi_{\text{cr}}) = 0$ (see Fig. 4). For angles $\Omega \in (\Omega_{\text{cr}}; \pi)$ that have a saddle point, one may expect, in the case of weak exchange interaction and strong magnetic dipolar interaction, the presence of a domain wall along the angle bisectrix which starts at the angle vertex and terminates at the point ξ_{cr} .

Analytic estimates of the position of a saddle point can be executed in two limiting cases. If $\Omega \lesssim \pi$, then the critical distance $\xi_{\text{cr}} \ll 1$, and the asymptotic estimation

$$\xi_{\text{cr}} \approx \frac{2}{e} e^{(\pi - \Omega/2) \text{ctg} \Omega} \quad (7)$$

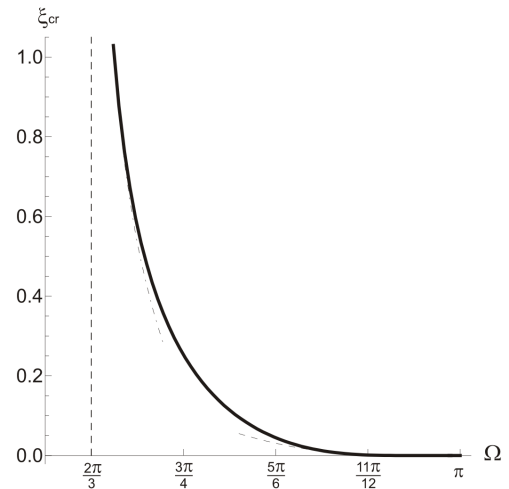


Fig. 4. Distance from the angle vertex to the saddle point as a function of the angle. The dashed and dash-dotted lines show estimates (7) and (8), respectively

is valid. In the opposite case $\Omega \gtrsim \Omega_{\text{cr}}$, the characteristic distance $\xi_{\text{cr}} \gg 1$, for which we have

$$\xi_{\text{cr}} \approx \frac{C_1}{\sqrt{\Omega - \Omega_{\text{cr}}}} + C_2 \sqrt{\Omega - \Omega_{\text{cr}}},$$

$$C_1 \approx 0,31, \quad C_2 \approx -0,882. \quad (8)$$

It should also be noted that the continual calculation presented in this section can turn out erroneous for the vertices of very acute angles; such problems require a separate consideration with regard for the discrete structure of a magnetic.

3. Effective Anisotropy for Regular Polygons

The above-executed analysis of the effective anisotropy near angles can be generalized to the solution of the problem concerning the effective anisotropy for regular polygons. Such an analysis is key for solving the problem on the distribution of magnetization in nanomagnetism in the form of polygons with regard for the magnetic dipolar interaction.

Let us consider a regular N -gon with thickness h , for which the distance from the center to an angle vertex is a . The calculation by formula (3b) gives the following expression for the coefficient of effective anisotropy:

$$\mathcal{B}(\rho, \chi) = -\frac{1}{2\pi} \left[\int_{\psi_0 - \varphi_0}^{\psi_0} F(P_0/h) e^{-2i\alpha} d\alpha + \right.$$

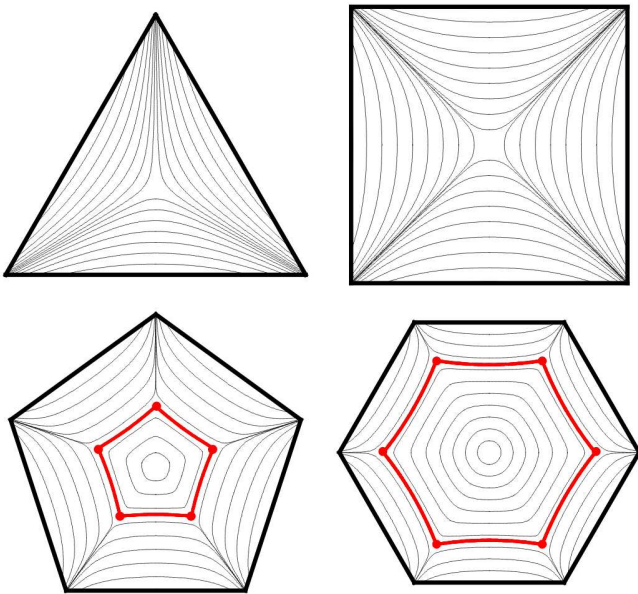


Fig. 5. Numerically calculated lines of effective anisotropy for certain regular polygons. The calculation is executed by formulas (9). The bold line shows the separatrix curve which passes through saddle points and separate the regions with different distributions of the lines of effective anisotropy, which can induce, in the presence of the strong magnetic dipolar interaction, different magnetization patterns: a state of the vortical type and a domain structure will be formed inside and outside, respectively. For all polygons, $h = a/2$

$$+ \sum_{k=1}^{N-1} \int_{\psi_{k-1}}^{\psi_k} F(P_k/h) e^{-2i\alpha} d\alpha \Big],$$

$$F(x) = G(x) + 2 \ln G(1/x);$$

$$P_n = \frac{a_n a_{n+1} b^{-1} \sin \varphi_n}{\cos[\alpha + \chi - (2n + 1)\pi/N]}, \quad n = \overline{0, N-1};$$

$$\psi_0 = -\arcsin \left[\frac{a_0}{b} \sin \varphi_0 \right], \quad b = 2a \sin(\pi/N),$$

$$\psi_j = \psi_0 + \sum_{i=1}^j \varphi_i, \quad j = \overline{1, N-1};$$

$$\varphi_m = \arccos \frac{a_m^2 + a_{m+1}^2 - b^2}{2a_m a_{m+1}}, \quad m = \overline{0, N-1};$$

$$a_k = \sqrt{\rho^2 + a^2 - 2\rho a \cos(\chi - 2\pi k/N)}, \quad k = \overline{0, N}. \quad (9)$$

In the calculation of (9), it was assumed that the origin of the system of coordinates (ρ, χ) coincides with

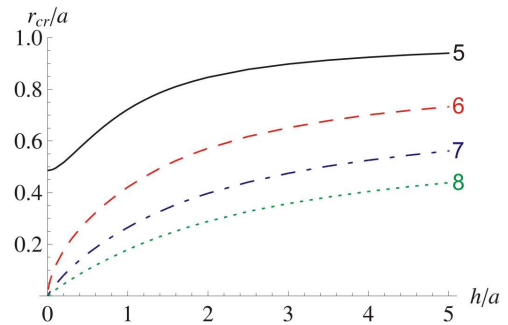


Fig. 6. Distance r_{cr} from the saddle point to the vertex of a polygon as a function of its thickness by the results of the numerical integration of relations (9). Different lines correspond to different polygons. The number of angles is denoted by a number on the right

the polygon center, and the angle χ is reckoned in the positive direction from the line connecting the polygon center with one of its vertices. Lines of effective anisotropy numerically calculated by formulas (9) for certain regular polygons are presented in Fig. 5.

In the previous section, it was established that a saddle point arises for planar angles $\Omega > \Omega_{cr} = 2\pi/3$, which coincides with the angle of a regular 6-gon. However, the calculation by formulas (9) testifies that, for bounded polygons, a saddle point appears already in 5-gons ($\Omega_5 = 3\pi/5$) (see Fig. 5). The saddle points are positioned on the bisectrices of angles of an N -gon. The distance r_{cr} from the saddle point to the vertex depends on the thickness of a polygon, and this dependence for $N > 5$ is the same: for infinitely thin magnetics, $r_{cr} \rightarrow 0$, and $r_{cr} \rightarrow a$ for thick ones (see Fig. 6). For 5-gons, $r_{cr} \rightarrow 0.49a$ as $h \rightarrow 0$, which is obviously a consequence of the fact that the angle of a 5-gon $\Omega_5 < \Omega_{cr}$ (see Fig. 6). These results are obtained numerically.

It should be recalled that the presented distributions of the lines of effective anisotropy are true only in the absence of a dependence of the magnetization on the coordinate normal to the plane of a magnetic. This condition can be violated at $h \gg \ell$.

Figures 5 and 6 show the distributions of directions of the lines of effective anisotropy. The quantitative values of the quantity \mathcal{B} , being the coefficient of effective uniaxial anisotropy whose direction is determined from the indicated figures, are given in Fig. 7 (case $N = 6$).

It is worth noting that if the distance from the saddle point to a vertex equals several interatomic distances, then the models accounting the discreteness of a crystalline structure and surface effects of a magnet

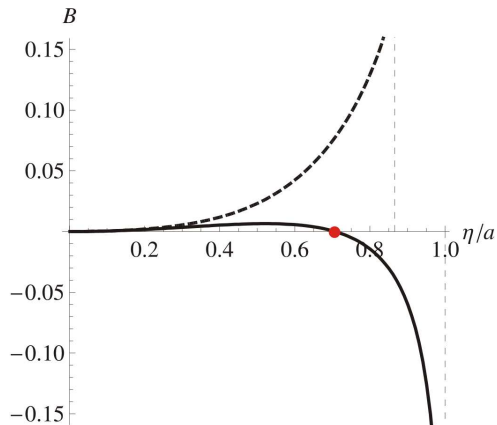


Fig. 7. Values of the coefficient B as a function of the distance from the 6-gon center along different directions. The solid line – along the diagonal, and the dashed line – in the direction normal to a side. The circle denotes the saddle point

should be used in the calculation of the magnetization distribution near the angle vertex.

4. Estimation of Sizes of the Magnetization Inhomogeneity Near Inhomogeneities of a Surface

The magnetization distribution in a nanoparticle near its lateral surface is very sensitive to surface roughnesses, which affects the dynamics of the process of remagnetization [21, 22]. This hampers the development of memory devices on the base of nanomagnetics, because it is quite difficult to control surface roughnesses on the fabrication of particles with submicron sizes. Therefore, it is practically interesting to estimate the sizes of a region near the lateral surface of a particle, where the state is essentially different from that in the bulk.

In this section, we consider particles which are in a vortex state. For simplicity, we will analyze a purely planar vortex state with

$$\theta = \pi/2, \quad \phi = \chi \pm \pi/2. \quad (10)$$

The energy density of the magnetic dipolar interaction in approximation (2) for a planar vortex (10) along the angle bisectrix $W^{\text{vor}} = \mathcal{A}(\xi) - \mathcal{B}(\xi)$. Analogously, the energy density in a particle which is homogeneously magnetized normally to the plane of a specimen ($\theta = 0$) has the form $W^{\text{uni}} = -2\mathcal{A}(\xi)$. The analysis testifies that the homogeneous state is energy-gained as compared with the vortex one near the lateral surface ($\xi \ll 1$) for any angles $\Omega \in (0; \pi)$ (see Fig. 2). On the contrary,

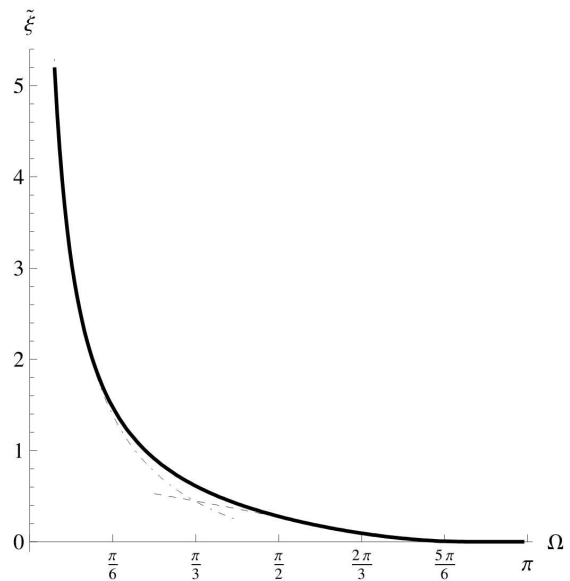


Fig. 8. Numerical solution of Eq. (11) as the upper bound for the size of the region in an angle Ω , where the magnetization goes out from the angle plane. The dash-dotted and dotted lines show estimates (12) and (13), respectively

as the distance from the angle vertex grows ($\xi \gg 1$), the vortex state becomes energy-gained ($W^{\text{vor}} < W^{\text{uni}}$). Thus, there exists the critical distance $\tilde{\xi}$ such that, at $\xi < \tilde{\xi}$, the quasihomogeneous orientation of the magnetization normally to the plane of a specimen becomes more favorable. The value of $\tilde{\xi}$ can be obtained as a solution of the equation $W^{\text{vor}} = W^{\text{uni}}$ or, what is the same,

$$3\mathcal{A}(\tilde{\xi}) = \mathcal{B}(\tilde{\xi}). \quad (11)$$

This equation can be analytically solved only in the limiting cases. For small angles ($\Omega \ll 1$), the characteristic size of inhomogeneities turns out to be significant ($\tilde{\xi} \gg 1$) and is approximately described by the formula

$$\tilde{\xi} \approx \frac{1}{\Omega} f^{-1}\left(\frac{1}{2}\pi(1 - \Omega^2/2)\right), \quad f(x) = x \left(1 - \ln \frac{x}{2}\right), \quad (12)$$

where f^{-1} denotes the function inverse to the function f . In the opposite case ($\Omega \lesssim \pi$), we have $\tilde{\xi} \ll 1$:

$$\tilde{\xi} \approx 2 \exp\left(-\frac{1}{1 - \Omega/\pi}\right). \quad (13)$$

The numerical solution of Eq. (11) is given in Fig. 8.

It is necessary to note that the obtained dependence $\tilde{\xi}(\Omega)$ gives only a rough upper bound for the size of the

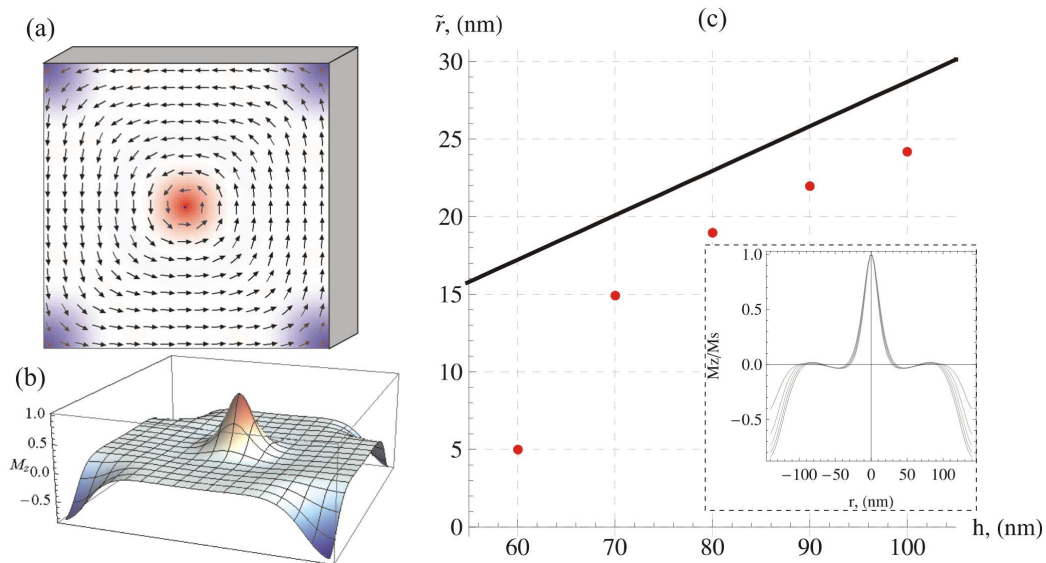


Fig. 9. (a) – the vortical distribution of the magnetization in a square prism (the degree of darkness characterizes the value of M_z ; (b) – the magnetization component M_z normal to the plane of the prism; (c) – the characteristic size of the inhomogeneity in the prism angle versus the prism thickness: symbols (filled circles) correspond to the results of micromagnetic modeling, the straight line $\tilde{r} = h\tilde{\xi}(\pi/2)$ presents the theoretical upper bound obtained from the solution of (11). In the insert, we show the quantity M_z along the prism diagonal (see the parameters in the text)

region near an angle on the surface, where the magnetization goes out from the particle plane. To obtain a more exact solution, it is necessary to solve the variational problem of minimization of the functional of energy. But the account of the exchange interaction energy in such a functional will lead to a decrease of the size of the region under consideration.

For the sake of illustration, we consider a right square prism. With the use of the software for micromagnetic modeling OOMMF [12], we obtained the vortex distributions of magnetization for prisms with different thicknesses. It is revealed that, in the angles of the prism, the magnetization component normal to the specimen plane (M_z) is nonzero. The maximum value of such a deviation of the quantity M_z , as well as the size of a region in which this deviation is concentrated, increases with the prism thickness. The values of M_z/M_s along the diagonal of the prism are given in the insert in Fig. 9. In the modeling, we took square prisms with the material parameters of permalloy ($A = 2.6 \times 10^{-12}$ J/m, $M_s = 8.6 \times 10^5$ A/m), the side length of 200 nm, and the thicknesses of 60, 70, 80, 90, and 100 nm. In Fig. 9, the profile with a greater amplitude of the deviation at the ends corresponds to a prism with greater thickness.

The filled circles in Fig. 9 show the distance from the angle vertex of the prism to a point on the bisectrix,

where the deviation of M_z is equal to M_s/e . Such a criterion is chosen due to the assumption about the Gauss form of deviations of $M_z(r)$. For the angle $\Omega = \pi/2$, the solution of Eq. (11) $\tilde{\xi}(\Omega) \approx 0.278$. In Fig. 9, we drew the straight line $\tilde{r} = h\tilde{\xi}(\pi/2)$. As is seen, even within such a rough model which does not account the exchange interaction and does not take a specific form of the inhomogeneity of $M_z(r)$ into account, we have obtained the upper bound of the inhomogeneity size which coincides by the order of magnitude with the values obtained by modeling.

5. Conclusions

By using the method of effective anisotropy caused by the magnetic dipolar interaction, we have theoretically studied the equilibrium distributions of the magnetization in thin magnetic nanoparticles of various forms. In particular, for a plane specimen in the form of an angle, we have revealed that the distribution of the lines of anisotropy is qualitatively changed on the passage through the critical angle $\Omega_{cr} = 2\pi/3$. For angles $\Omega \in (\Omega_{cr}; \pi)$, there appears a saddle point which can be joined with the angle vertex by a domain wall in the case of weak exchange interaction.

For the magnetics with finite sizes, a closed separatrix curve arises instead of a single saddle point. In the interior region of this curve, a vortex state can be formed under the condition of weak exchange interaction, whereas an N -domain structure arises outside it. It is established that the separatrices appear in the polygons, the number of angles in which is not less than 5. The sizes of a separatrix depend on the thickness of a magnetic. We have also shown that, near the angle vertex, the appearance of the magnetization component normal to the specimen plane is energy-gained. The comparison with the results of micromagnetic simulations for square prisms indicates that the obtained theoretical estimates can be considered as the upper bound of the sizes of inhomogeneities of the magnetization which are observed near the angle vertices.

The authors thank Prof. Yu.B. Gaididei for useful discussions. The work was supported by the grant No. F25.2/081 of the State Fund for Fundamental Studies of Ukraine.

1. A. Hubert and R. Schäfer, *Magnetic Domains: the Analysis of Magnetic Microstructures* (Springer, Berlin, 1998).
2. R. Skomski, *J. Phys. C* **15**, R841 (2003).
3. S.D. Bader, *Rev. Mod. Phys.* **78**, 1 (2006).
4. E. Stoner and E. Wohlfarth, *Philosophical Transactions of the Royal Society of London. Series A, Mathematical and Physical Sciences* (1934–1990) **240**, 599 (1948).
5. J. Stöhr and H. C. Siegmann, *Magnetism: From Fundamentals to Nanoscale Dynamics, vol. 152 of Springer Series in solidstate sciences* (Springer, Berlin–Heidelberg, 2006).
6. H. A. M. van den Berg, *J. Appl. Phys.* **57**, 2168 (1985).
7. H.A.M. van den Berg, *J. Appl. Phys.* **60**, 1104 (1986).
8. H.A.M. van den Berg and A.H.J. van den Brandt, *J. Appl. Phys.* **62**, 1952 (1987).
9. H.A.M. van den Berg, *J. Appl. Phys.* **61**, 4194 (1987).
10. R. Hertel, O. Fruchart, S. Cherifi, P.-O. Jubert, S. Heun, A. Locatelli, and J. Kirschner, *Phys. Rev. B* **72**, 214409 (2005).
11. R.P. Cowburn, *J. Magn. Magn. Mater.* **242–245**, 505 (2002).
12. The Object Oriented MicroMagnetic Framework, developed by M.J. Donahue and D. Porter mainly, from NIST. We used the 3D version of the 1.2 α 2 release, URL <http://math.nist.gov/oommf/>.
13. G. Gioia and R.D. James, *Proc. R. Soc. Lond. A* **453**, 213 (1997).
14. B.A. Ivanov and C.E. Zaspel, *Appl. Phys. Lett.* **81**, 1261 (2002).
15. G. Carbou, *Math. Models and Methods in Appl. Sci. (M3AS)* **11**, 1529 (2001).
16. K.Y. Guslienko, S.O. Demokritov, B. Hillebrands, and A.N. Slavin, *Phys. Rev. B* **66**, 132402 (2002).
17. V.E. Kireev and B.A. Ivanov, *Phys. Rev. B* **68**, 104428 (2003).
18. R.V. Kohn and V.V. Slastikov, *Archive for Rational Mechanics and Analysis* **178**, 227 (2005).
19. O. Tchernyshyov and G.-W. Chern, *Phys. Rev. Lett.* **95**, 197204 (2005).
20. J.-G. Caputo, Y. Gaididei, V.P. Kravchuk, F.G. Mertens, and D.D. Sheka, *Phys. Rev. B* **76**, 174428 (2007).
21. Y. Zheng and J.-G. Zhu, *J. Appl. Phys.* **81**, 5471 (1997).
22. T.-N. Fang and J.-G. Zhu, *J. Appl. Phys.* **87**, 7061 (2000).

Received 14.12.07.

Translated from Ukrainian by V.V. Kukhtin

ЕФЕКТИВНА МАГНІТОДИПОЛЬНА АНІЗОТРОПІЯ НАНОМАГНІТИКІВ: РІВНОВАЖНІ КОНФІГУРАЦІЇ НАМАГНІЧЕНОСТІ

В.П. Кравчук, Д.Д. Шека

Резюме

Теоретично досліджено рівноважні розподіли намагніченості в тонких магнітних наночастинках різноманітної форми в наближенні ефективної анізотропії, зумовленої магнітодипольною взаємодією. Передбачено розподіл намагніченості поблизу плоского кута та для тонких магнетиків у формі правильних багатокутників за умов слабкої обмінної взаємодії. Проведено теоретичний аналіз розмірів неоднорідностей у розподілі намагніченості поблизу вершини кута. Аналітичні результати добре узгоджуються з даними мікромагнітного моделювання для квадратної призми.